COB-2021-0404
ENERGY HARVESTING FROM CHAOTIC VIBRATION

Luã Guedes Costa
Eduardo Villela Machado dos Reis
Marcelo Amorim Savi
Universidade Federal do Rio de Janeiro, COPPE, Department of Mechanical Engineering, Center for Nonlinear Mechanics
guedes@mecanica.coppe.ufrj.br
eduardovillela@mecanica.coppe.ufrj.br
savi@mecanica.ufrj.br

Abstract. *Recent developments in technology requires the employment of self-powered sensors, actuators and small electronic devices. Energy harvesting systems are useful to this goal and can be configured in many different ways to improve process efficiency. The converted energy can also be stored to be further consumed. Mechanical vibration is one of the energy sources that can be converted into electrical energy. Besides the energy harvested, it is possible to mitigate undesirable vibrations. Smart materials are usually employed in these systems in order to promote electro-mechanical conversion. Piezoelectrics are smart materials employed to several applications in industry. Nonlinear characteristics are usually exploited in order to enhance energy harvesting capacity. In this regard, multistable energy potential is usually exploited by adding magnetic interactions to the system, being described by a Duffing-type system. Duffing oscillator has a rich dynamical behavior including chaos. In this regard, nonlinear dynamics analysis is essential for a proper design of the energy harvesting system. An important issue to be investigated is the correlation between energy harvesting capacity and the kind of response, which makes essential the use of proper nonlinear tools for a deep dynamical analysis. This paper addresses the correlation between the maximum Lyapunov exponent and power harvesting parameters in order to define harvesting capacity. Among the possibilities to be investigated, it should be highlighted the output RMS power and the efficiency of the energy conversion. This analysis allows one to connect the degree of chaoticity, represented by the value of Lyapunov exponents, with the electro-mechanical conversion efficiency.*

Keywords: Energy Harvesting, Nonlinear Vibration, Chaos, Lyapunov Exponent, Bistable Systems

1. INTRODUCTION

Vibration-based energy harvesting has been an emergent research subject over the last few decades. The main idea is to convert wasted vibration energy into useful electrical energy through some electro-mechanical mechanism. For this purpose, synthetic piezoelectric materials are often a good alternative due to their capacity of converting strain energy into electrical energy through the direct piezoelectric effect. Applications are vast and versatile as: civil structures (Erturk, 2011; Peigney and Siegert, 2013; Zuo and Tang, 2013; Xiang *et al.*, 2014; Elhalwagy *et al.*, 2017; Wang *et al.*, 2018), biomedic applications (Dagdeviren *et al.*, 2014), raindrop impacts (Ilyas and Swingler, 2015; Bao and Wang, 2021), self powered wireless sensors and MEMs (Noël E. duToit *et al.*, 2006; Lee and Choi, 2014), offshore applications (Nabavi *et al.*, 2018), vehicles (Zhang *et al.*, 2018; Tian *et al.*, 2020), among others.

Early developments show that conventional piezoelectric energy harvester devices are efficient only in a small bandwidth, on the vicinity of the system natural frequency. Therefore, slight changes on the ambient vibration dramatically reduces the output power from the harvester (Erturk and Inman, 2011b). This characteristic implies limited applications in real world situations as natural vibrations are often composed by multiple frequency bands. In order to deal with this problem, new researches began to emerge showing that nonlinear energy harvesting devices can effectively broaden the bandwidth of operation (Pellegrini *et al.*, 2013). In this regard, bistable energy harvesters were one of the first nonlinear devices to be investigated (Stanton *et al.*, 2009; Ferrari *et al.*, 2010a,b; Erturk and Inman, 2011a).

Bistable energy harvester systems are known to produce two patterns of motion: intra-well motion, in which the dynamics of the system is trapped in a energy well around one stable equilibrium point; and inter-well motion, in which the dynamics of the system freely oscillates around two equilibrium points (Tran *et al.*, 2018). Although periodic motion, generally, is the best alternative for energy harvesting purposes, it should be pointed out that inter-well chaotic behavior is more interesting than intra-well periodic behavior and therefore, beneficial chaotic motion can increase the output power of the system compared to the conventional harvesters. Regarding that, Costa *et al.* (2021) introduces the concept of

intensity of inter-well motion, represented by IW(%), accounting the percentage of cycles that the system visits two equilibrium points during steady state. On this basis, it is often possible to establish that the greater is IW(%), the greater is the output power of the system.

This paper addresses a numerical investigation of Duffing-type energy harvesting systems, establishing a correlation among the maximum Lyapunov Exponent (λ_1), the intensity of inter-well motion (IW(%)) and the energy harvesting performance for chaotic dynamics in general . Bistable behavior is of concern and results show interesting situations to be exploit for energy harvesting purposes.

2. THEORETICAL BACKGROUND

Energy harvesting system is typically represented by a piezomagnetoelastic device composed by a composite cantilever beam formed by one layer of a structural material and two layers of a synthetic piezoelectric material (Figure 1a). The bistablity of the system is induced by magnetic interactions, generating a unstable equilibrium point at the center line of the beam and two opposite stable equilibrium points associated with a double well potential.

(a)   (b)
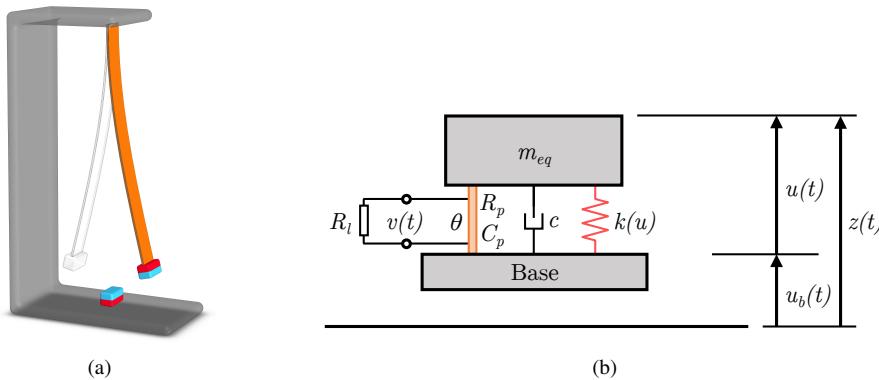
Figure 1: (a) Piezomagnetoelastic device, an example of a bistable energy harvesting structure. (b) Corresponding lumped model.

The system mathematical model is established by considering the first vibration mode of the piezomagnetoelastic beam, being represented by an electro-mechanical oscillator presented in Figure 1b. The governing equations of the system are given by(Erturk and Inman, 2011b; Paula *et al.*, 2015; Costa *et al.*, 2021):

$$m_{\text{eq}}\ddot{u} + c\dot{u} + \mathfrak{f}(u) - \theta v = -m_{\text{eq}}\ddot{u}_b$$
$$C_p\dot{v} + \frac{1}{R_{\text{eq}}}v + \theta\dot{u} = 0 \tag{1}$$

where $\mathfrak{f}(u) = -au + bu^3$ is the system's restitution force, where $(a, b) > (0, 0)$ are the restitution parameters. u and v represents the displacement and voltage, respectively. The harvester is excited by a harmonic base excitation of the type $u_b = A\sin(\omega t)$, and over dot notation $\dot{()} = d()/dt$ represents time derivative, thus the base acceleration is $\ddot{u}_b = -A\omega^2\sin(\omega t)$. The equivalent mass and the damping of the system are m_{eq} and c, respectively, whilst C_p and R_{eq} are the electrical parameters related to the capacitance of the piezoelectric element and the equivalent electrical resistance of the system, respectively. The equivalent electrical resistance of the system is composed by the electrical resistance of the circuit (R_l) and the electrical resistance of the piezoelectric element (R_p). Finally, θ is the electro-mechanical coupling coefficient of the piezoelectric element that couples the mechanical behavior with the electrical response.

Stability analysis of the system shows the emergence of 3 equilibrium points, EP, of the form $(\bar{u}, \bar{u}')$, being two of them stable and one unstable, as follows:

$$\text{EP}_1 \text{ (stable)} = \left(-\sqrt{\frac{a}{b}}, 0\right), \qquad \text{EP}_2 \text{ (unstable)} = (0, 0), \qquad \text{EP}_3 \text{ (stable)} = \left(\sqrt{\frac{a}{b}}, 0\right) \tag{2}$$

Dimensionless equations are conveniently employed, being defined in the sequence. The half distance between system equilibrium states is used as a characteristic length ($L = \sqrt{a/b}$). Besides, the oscillation frequency around one of the stable configurations is used to define a characteristic time ($\omega_0 = \sqrt{2a/m_{\text{eq}}}$). Finally, the voltage amplitude achieved when the beam oscillates with amplitude $\sqrt{a/b}$ and $R_{\text{eq}} \to \infty$ is employed to defined a characteristic voltage. Under these assumptions, the following definitions are presented:

$$x = \frac{u}{L} = \sqrt{\frac{b}{a}}u, \qquad \tau = \omega_0 t = \sqrt{\frac{2a}{m_{\text{eq}}}}t, \qquad \nu = \frac{C_p}{\theta}\sqrt{\frac{b}{a}}v, \tag{3}$$

where x, τ, ν are the dimensionless displacement, time and voltage, respectively. Dimensionless time derivatives are defined using the chain rule as:

$$\dot{x} = \frac{dx}{d\tau} = \frac{dx}{dt}\frac{dt}{d\tau} = \frac{1}{\omega_0}\sqrt{\frac{b}{a}}\dot{u} \tag{4}$$

$$\ddot{x} = \frac{d\dot{x}}{d\tau} = \frac{d\dot{x}}{dt}\frac{dt}{d\tau} = \frac{1}{\omega_0^2}\sqrt{\frac{b}{a}}\ddot{u} \tag{5}$$

$$\dot{\nu} = \frac{d\nu}{d\tau} = \frac{d\nu}{dt}\frac{dt}{d\tau} = \frac{C_p}{\theta\omega_0}\sqrt{\frac{b}{a}}v \tag{6}$$

Based on that, the dimensionless equations of motion are given by:

$$\ddot{x} + 2\zeta\dot{x} + \frac{1}{2}(-x + x^3) - \chi\nu = \gamma\sin(\Omega\tau)$$
$$\dot{\nu} + \varphi\nu + \dot{x} = 0 \tag{7}$$

where dimensionless parameters arise as ζ being the damping coefficient, χ the electro-mechanical coefficient in the mechanical equation, φ a coefficient proportional to the electrical resistance; Ω and γ are respectively the dimensionless forcing frequency and amplitude:

$$\zeta = \frac{c}{2\sqrt{2am_{\text{eq}}}}, \qquad \chi = \frac{\theta^2}{2aC_p}, \qquad \Omega = \frac{\omega}{\omega_0}, \qquad \gamma = A\sqrt{\frac{b}{a}}\Omega^2, \qquad \varphi = \frac{1}{\omega_0 C_p R_{\text{eq}}}. \tag{8}$$

The energy harvesting characterization needs the definition of the input power from base excitation and the the output power converted to electrical energy by the piezoelectric material. Since each term in Eq. 7a has force dimension, when multiplied by $\dot{x}$ it turns into power dimension. This way, in order to obtain expressions for such sought powers, one multiplies it by $\dot{x}$ and integrates in time domain from $\tau = \tau_0$ to $\tau = \tau_f$, which yields

$$\int_{\tau_0}^{\tau_f}\left[\ddot{x} + 2\zeta\dot{x} - \frac{x}{2} + \frac{x^3}{2} - \chi\nu\right]\dot{x}\,d\tau = \int_{\tau_0}^{\tau_f}\left[\gamma\sin(\Omega\tau)\right]\dot{x}\,d\tau \tag{9}$$

After substituting Eq. 7b into Eq. 9, integrating by parts and algebraic manipulation, one obtains the following equation

$$\left[\frac{\dot{x}^2}{2} - \frac{x^2}{4} + \frac{x^4}{8} + \frac{\chi\nu^2}{2}\right]_{\tau_0}^{\tau_f} = \int_{\tau_0}^{\tau_f}\gamma\dot{x}\sin(\Omega\tau)\,d\tau - \int_{\tau_0}^{\tau_f}2\zeta\dot{x}^2\,d\tau - \int_{\tau_0}^{\tau_f}\chi\varphi\nu^2 d\tau \tag{10}$$

where the first term in the right hand side of Eq. 10 stands for the work done by the base into the system, the second for the dissipated energy by the damper and, finally, the last one for the piezoelectric energy harvested in the time interval $[\tau_0, \tau_f]$. Each integrand from these three terms, naturally, yields each respective power expression. At this point, one should notice that, if the system displays a periodic response with period $\tau_f - \tau_0$, the left hand side of Eq. 10 becomes null. Therefore, one concludes that all the work done by the base excitation is dissipated either by the damper or the electrical circuit during one period cycle. Moreover, since the integrand from both dissipation terms are always positive, their integral from Eq. 10 becomes larger as the difference $\tau_f - \tau_0$ also becomes larger. Considering a bounded response for both x and ν, the left hand side of Eq. 10 does not grow as the difference $\tau_f - \tau_0$ grows. This way, the only term that can balance the large values of both dissipation terms are the work done by the base excitation. From this physical discussion, considering the limit $\tau_f - \tau_0 \to \infty$, Eq. 10 becomes

$$\lim_{\tau_f - \tau_0 \to \infty}\left[\int_{\tau_0}^{\tau_f}\gamma\dot{x}\sin(\Omega\tau)\,d\tau - \int_{\tau_0}^{\tau_f}2\zeta\dot{x}^2\,d\tau - \int_{\tau_0}^{\tau_f}\chi\varphi\nu^2 d\tau\right] = 0 \tag{11}$$

Therefore, the input power from base excitation, P_{in}, and the out power, harvested by the electrical circuit, P_{out}, are given by

$$P_{\text{in}} = \gamma\dot{x}\sin(\Omega\tau)$$
$$P_{\text{out}} = \chi\varphi\nu^2 \tag{12}$$

Thus, in accordance with the literature, one can assume the energy harvesting efficiency η to be the ratio between the Root Mean Square (RMS) of P_{in} over P_{out}, yielding

$$P_{\text{in}}^{\text{RMS}} = \frac{1}{\tau_f - \tau_0} \int_{\tau_0}^{\tau_f} P_{\text{in}}^2 \, \mathrm{d}\tau \tag{13}$$

$$P_{\text{out}}^{\text{RMS}} = \frac{1}{\tau_f - \tau_0} \int_{\tau_0}^{\tau_f} P_{\text{out}}^2 \, \mathrm{d}\tau \tag{14}$$

$$\eta = \frac{P_{\text{out}}^{\text{RMS}}}{P_{\text{in}}^{\text{RMS}}} \tag{15}$$

3. AN OVERVIEW OF THE SYSTEM DYNAMICS

The bistable Duffing-type oscillator is characterized by straight unstable equilibrium configuration and two stable and symmetrical configurations in the vicinity of the straight configuration. Depending on the base excitation, the system can oscillate around one of the stable equilibrium configurations, which is called intra-well oscillation, or can oscillate around both stable configurations, yielding an inter-well oscillation. It is worthwhile mentioning that, either periodic or chaotic responses can be associated with each one of these behaviors. The measurement of the intensity of the inter-well oscillation is of major importance as the greater the intensity of inter-well motion, greater the RMS output power tends to become (Costa $et\ al.$, 2021). Therefore, it can be evaluated by the ratio between the number of jumps between stable equilibrium points (J) the system exhibits in steady state, and the maximum jumps between stable equilibrium points (J_{max}) the system is generally capable of performing in the steady state time interval, as follows:

$$\text{IW} = \frac{J}{J_{\text{max}}} \tag{16}$$

A dynamical jump (J) can be illustrated by the point of view of the dimensionless mechanical restitution force of the system, $f(x) = -\dfrac{x}{2} + \dfrac{x^3}{2}$, that results in the dimensionless potential mechanical energy of the system, $U(x) = -\dfrac{x^2}{4} + \dfrac{x^4}{8}$, also represented by the mechanical portion of the left hand side of Eq. 9. Figure 2 shows the shapes of the mechanical restitution force, the mechanical potential energy function and the path the system has to course to execute a jump. A jump occurs when the system travels from the first stable equilibrium position to the second stable equilibrium position, or vice-versa. For that, the system needs to have enough energy to overcome a potential energy barrier that has its peak at the unstable equilibrium position. For this reason, sometimes it can be trapped in a potential well, due to the lack of energy needed to overcome the barrier, producing transitory intra-well motion, diminishing the intensity of total inter-well motion (IW).
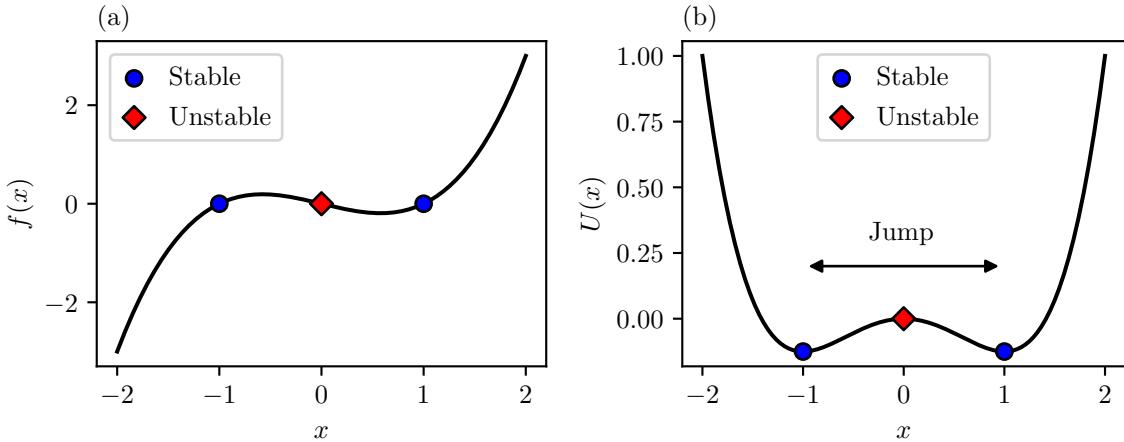

Figure 2: (a) Dimensionless mechanical restitution force of the system, $f(x)$. (b) Dimensionless mechanical potential energy function of the system, $U(x)$. Blue circle shaped markers represent stable equilibrium points, while diamond shaped red markers represent the unstable equilibrium point.

Preliminary results, shown in Figure 3, illustrate this kind of behavior. Parameters employed on this analysis are summarized as follows: $\zeta = 0.025$, $\chi = 0.0125$, $\varphi = 0.035$, $\gamma = 0.3$, $x(0) = 1$, $\dot{x}(0) = \nu(0) = 0$, and Ω changes according to the curve. The black curve ($\Omega = 1.3$) shows a situation in which the system is trapped in a energy potential well, producing intra-well motion, therefore IW = 0%. Still, the blue curve ($\Omega = 1.18$) shows a chaotic dynamics in which the system is in a transitory inter-well motion with intensity of IW = 25.4% and is producing more voltage than the previous situation. Additionally, purple ($\Omega = 0.3$) and dark gray ($\Omega = 1.052$) curves show dynamical motions that produces similar voltage outputs and present a full inter-well motion (IW = 100%). These example illustrates how

chaotic motion can be beneficial by the point of view of energy generation, and sometimes be comparable or better than periodic motions, depending on the situation. On this case, the periodic full inter-well motion (IW = 100%) is better than the chaotic with transitory inter-well motion (IW = 25.4%), however it can be comparable with the chaotic full inter-well dynamics (IW = 100%); on the other hand the periodic intra-well dynamics (IW = 0%) is the worst in terms of energy harvested. The illustrated phenomena shows the need of a more careful analysis of the chaotic dynamics of bistable systems for energy harvesting purposes.
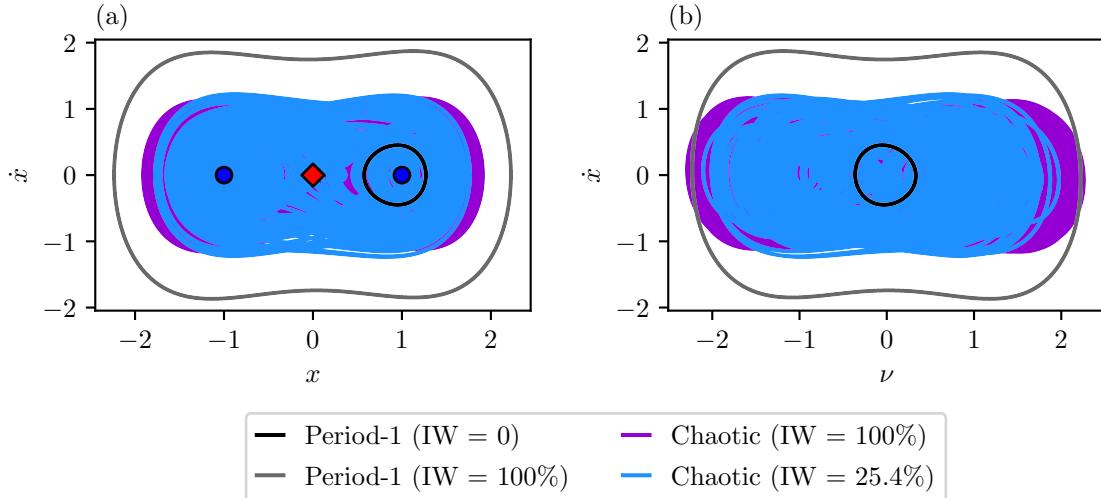

Figure 3: (a) Steady state x-$\dot{x}$ phase space for different dynamical responses and IW intensities. (b) Steady state ν-$\dot{x}$ phase space for different dynamical responses and IW intensities. Blue circle shaped markers represent stable equilibrium points, while diamond shaped red markers represent the unstable equilibrium point.

From this point on, the dimensionless parameters employed in all analysis are given in Table 1. The electrical parameters are kept constant in all simulations, while mechanical parameters, such as damping ζ and base excitation parameters, are varied.

Numerical simulations are carried out employing fourth order Runge-Kutta method. A total of $n_p = 1000$ forcing periods are analyzed with initial conditions of $x(0) = 1, \dot{x}(0) = 0, \nu(0) = 0$. Also, three different cases considering different values of damping as $\zeta_1 = 0.0025$, $\zeta_2 = 0.025$ and $\zeta_3 = 0.25$ are chosen to determine the influence of mechanical dissipation on system response. The largest Lyapunov exponent λ_1 are employed to characterize chaos, being calculated by the method proposed by Wolf et $al.$ (1985). Lyapunov exponents are evaluated in two initial time stages, $\tau_0 = 0$ and $\tau_0 = 0.75\tau_f$ (steady state), and compared, in order to ensure proper convergence on cases that show long transient chaos orbits, where $\tau_f = 2\pi n_p/\Omega$ is the final time of integration.

Table 1: Parameters employed in all numerical analyzes.

ζ	χ	φ	γ	Ω	$x(0)$	$\dot{x}(0)$	$\nu(0)$	n_p
$0.0025 \rightarrow 0.25$	0.0125	0.035	$0.01 \rightarrow 1$	$0.01 \rightarrow 2$	1	0	0	1000

Initially, the largest Lyapunov exponent (λ_1), intensity of inter-well motion (IW), $P_{\text{out}}^{\text{RMS}}$, and efficiency ($\eta$) diagrams are investigated considering the γ-Ω domain. These diagrams present an overview of the system dynamics for different orders of magnitude of damping coefficient ($\zeta = 0.0025, 0.025$ and 0.25) (Figure 4). The first row of diagrams considers the quantification of chaos by the analysis of the largest Lyapunov exponent λ_1. Chaotic responses are reckoned by displaying a positive Lyapunov exponent (rainbow colors on the colorbar scale), while periodic ones show a negative exponent (grayscale colors on the colorbar scale).

Since the focus is on the chaotic responses, the second, third and fourth rows of Figure 4 highlights only show the chaotic attractors, while periodic responses are overshadowed with black color. The second row shows the intensity of inter-well motion IW. It is observed that for the first two cases ($\zeta = 0.0025$ and $\zeta = 0.025$), low values of Ω present higher intensities, while for higher frequencies, IW shows more variation, presenting lower values. For the third case ($\zeta = 0.25$), results of IW are more complex, however still following the same pattern, indicating higher intensities for lower frequencies.
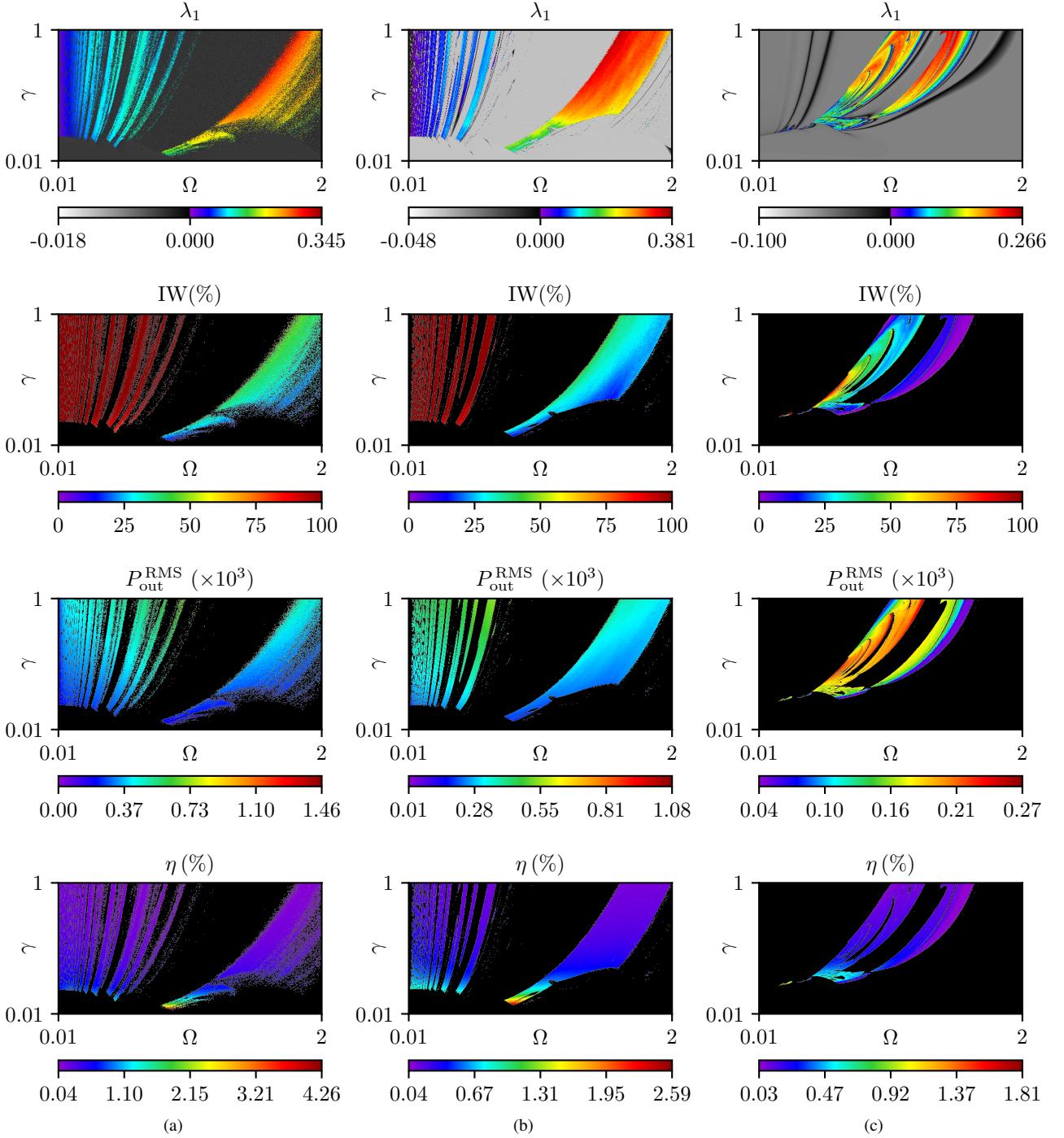
Figure 4: Different aspects of the system dynamics for (a) $\zeta = 0.0025$, (b) $\zeta = 0.025$, and (c) $\zeta = 0.25$. The first row represents the largest Lyapunov Exponent of the system; the second row represents the intensity of inter-well motion; the third row shows the RMS of output power, i.e. the converted energy; the fourth row exhibits the efficiency of the conversion.

The third row of Figure 4 shows the RMS output power, P_{out}. Results of the first two cases ($\zeta = 0.0025$ and 0.025) are difficult to distinguish variations because of few points with peak values at the top boundary of the chaotic region around the interval $1 < \Omega < 2$. The third case ($\zeta = 0.25$) indicates that the values of P_{out} present some degree of nonlinear proportionality with the values of IW and λ_1, however it is difficult to establish a proper correlation from these diagrams.

Efficiency diagrams presented on the fourth row show that the efficiency of conversion reaches its peak near the resonance peak and also indicates some correlation with the value of Lyapunov exponents. Moreover, it can be observed that the greater is the damping coefficient (ζ), the lower is the maximum efficiency of the system.

Results indicate that a simplification of the parameter domain is necessary to find the correlations between the quan-

tities of interest. From this point on, it is carried out an analysis of the energy harvesting parameters only for 100% inter-well oscillations (IW $= 100\%$). For cases where $0 < \text{IW} < 100$, the dynamics of the system proved to be much more richer and complex. Also, sets of values of forcing amplitude (γ) are chosen according to the analysis. The next section investigates the correlation among quantities of interest based on these simplifications.

4. CORRELATIONS AMONG QUANTITIES OF INTEREST

The analysis of a subset of fixed parameters is now in focus. Bifurcation diagrams are built in order to study the dynamics on specific cases. All parameters are constant and Ω is varied from 0.01 to 1. All simulations employ the initial conditions of $x(0) = 1$ and $\dot{x}(0) = \nu(0) = 0$ for each set of parameters.

Fig. 5 presents both $P_{\text{in}}^{\text{RMS}}$ and $P_{\text{out}}^{\text{RMS}}$, as well as the efficiency from the harvesting process η. As previously mentioned, the dynamical response can be either chaotic or periodic. Thus, results in Fig. 5 are displayed in different colors for each kind of response. One can observe that increasing the excitation frequency increases the amount of mechanical input power to the system. Since $\Omega = 1$ yields the natural frequency of an oscillation with small enough amplitude around on of the stable configurations, it is expected an increasing of input power as Ω increases towards $\Omega = 1$ due to larger amplitudes of oscillation. Moreover, for almost any fixed Ω, one can observe that $P_{\text{in}}^{\text{RMS}}$ is greater for chaotic responses than for periodic ones. However, the opposite takes place for $P_{\text{out}}^{\text{RMS}}$. In other words, a chaotic response allows the base excitation to furnish more work to the mechanical system when compared to a periodic response, but a smaller fraction of this work is truly converted into electrical power by the piezoelectric layer. The efficiency of the conversion can be observed in Fig. 5c, where one can see chaotic responses always show less efficiency.
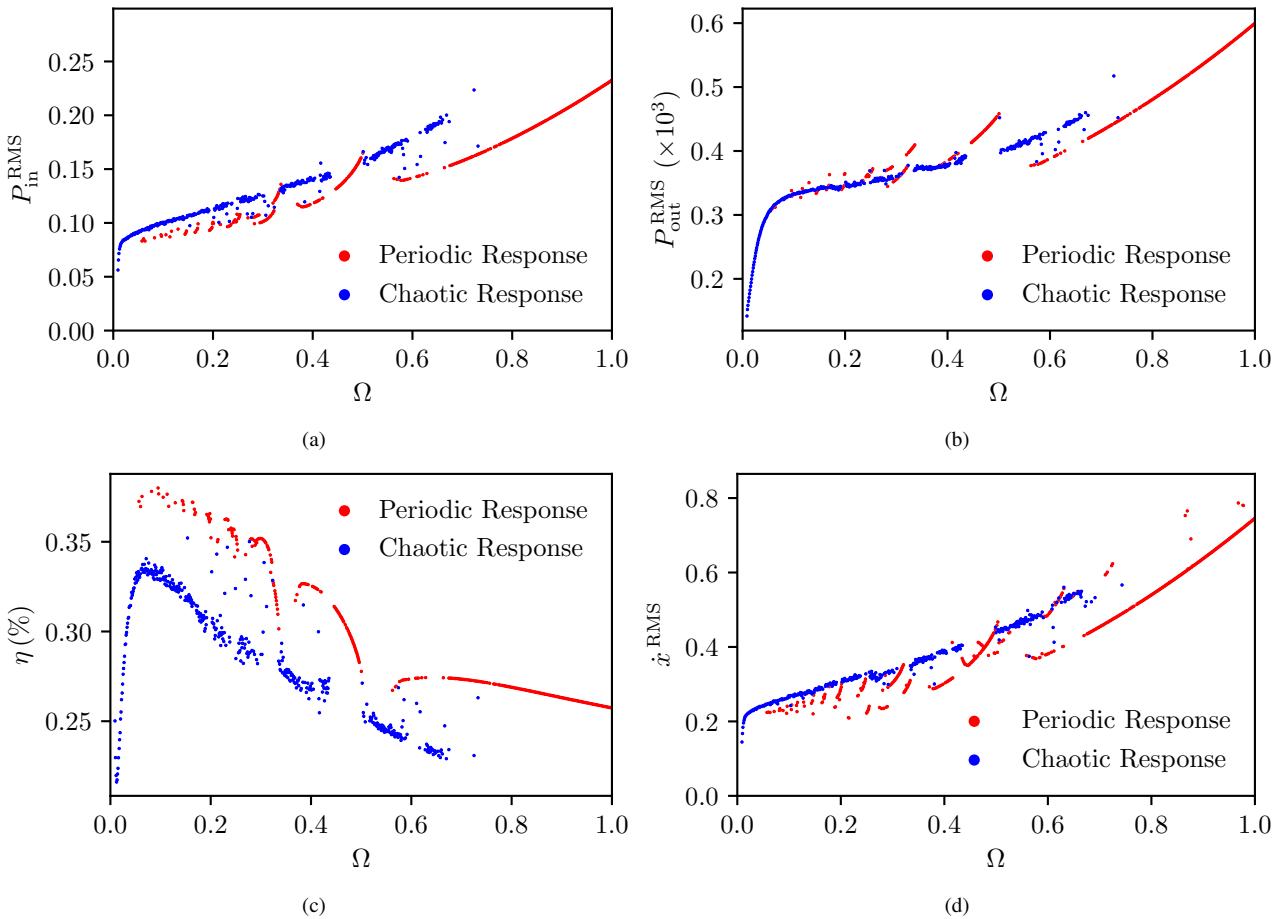

Figure 5: Bifurcation diagrams of (a) $P_{\text{in}}^{\text{RMS}}$, (b) $P_{\text{out}}^{\text{RMS}}$, (c) η, and (d) $\dot{x}^{\text{RMS}}$ for $(\zeta, \gamma) = (0.0025, 0.5)$.

Since the amount of input power from base excitation is greater for chaotic response, the RMS of velocity is also greater, which can be observed in Fig. 5. From Eq. 10 one observes that the power dissipated by damping effects is proportional to $\dot{x}^2$, which is also proportional to the RMS of the velocity ($\dot{x}^{\text{RMS}}$). Moreover, from Eq. 11 and 12b, the electric power is a function, although not exclusive, of $\dot{x}^2$. Therefore, both effects (damping and power conversion) compete to gain a wider fraction of the input power. For low values of Ω, the increase of Ω also increases the fraction of input power which is converted by the electric circuit ($P_{\text{out}}^{\text{RMS}}$), given by a positive slope $d\eta/d\Omega$. As Ω still increases, a

maximum efficiency value is reached, followed by a constant growing domination of input power fraction that is dissipated by the mechanical damper.

Fig. 6 displays the bifurcation diagram for λ_1, where it is possible to see that λ_1 continuously increases as Ω increases. This way, the rate a small enough perturbation grows increases as the excitation frequency approaches $\Omega = 1$.
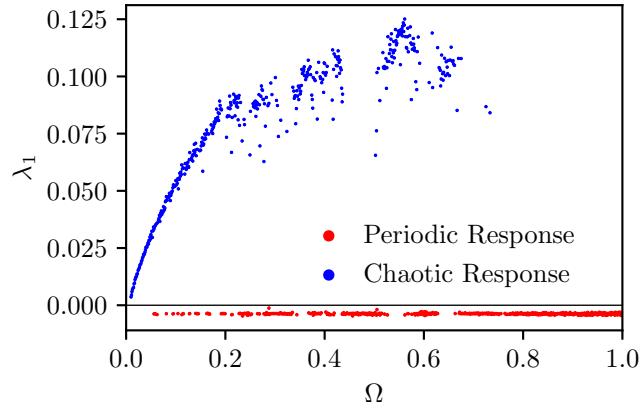

Figure 6: Bifurcation diagram of Lyapunov exponent λ_1 for chaotic responses (blue) and periodic (red).

Regarding the amplitude of excitation, Fig. 7 displays the influence of γ concerning the evaluation of the efficiency η and Lyapunov exponent λ only for chaotic responses. Besides the shape of all efficiency curves are the same, smaller γ can increase the efficiency of energy harvesting, although the purple curve, representing $\gamma = 0.25$, shows less amount of data because of lower number of points in which IW $= 100\%$ on this case. On the other hand, the Lyapunov exponent seemed to be not sensitive to γ variation. This way, despite the input power increases for higher values of γ, due to Eq. 12a, non intuitively the rate of divergence in phase space does not grow.
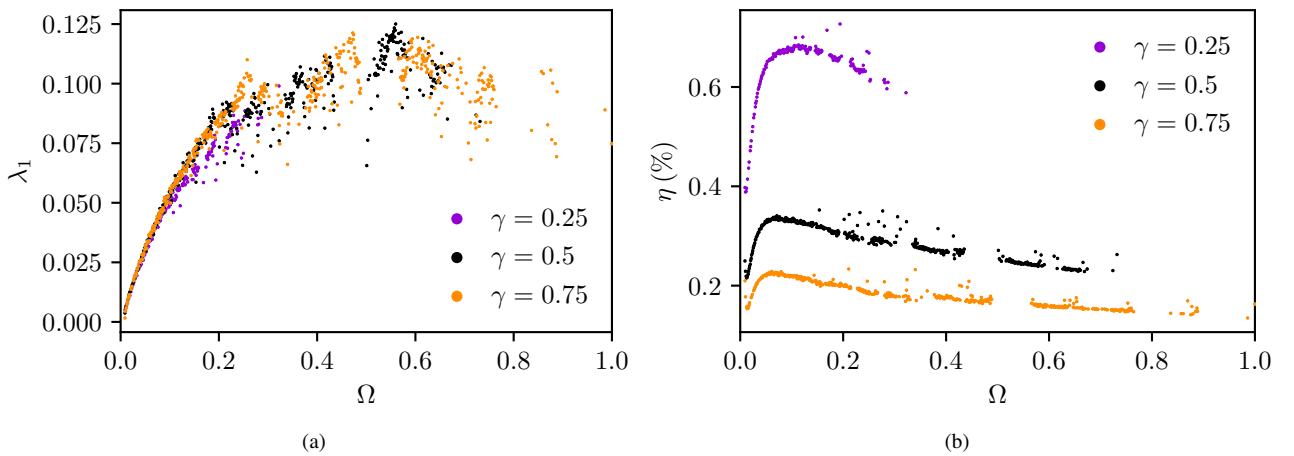

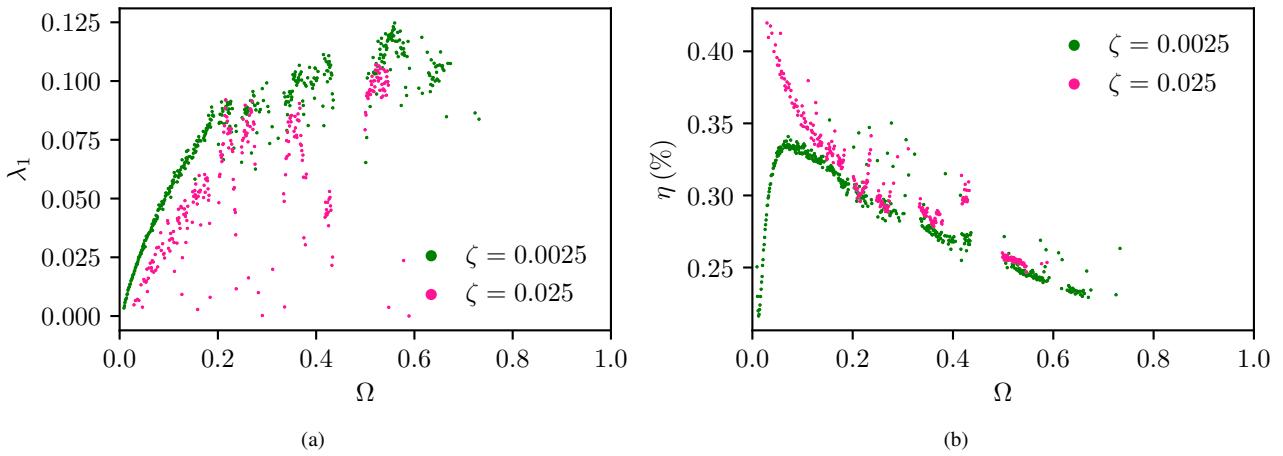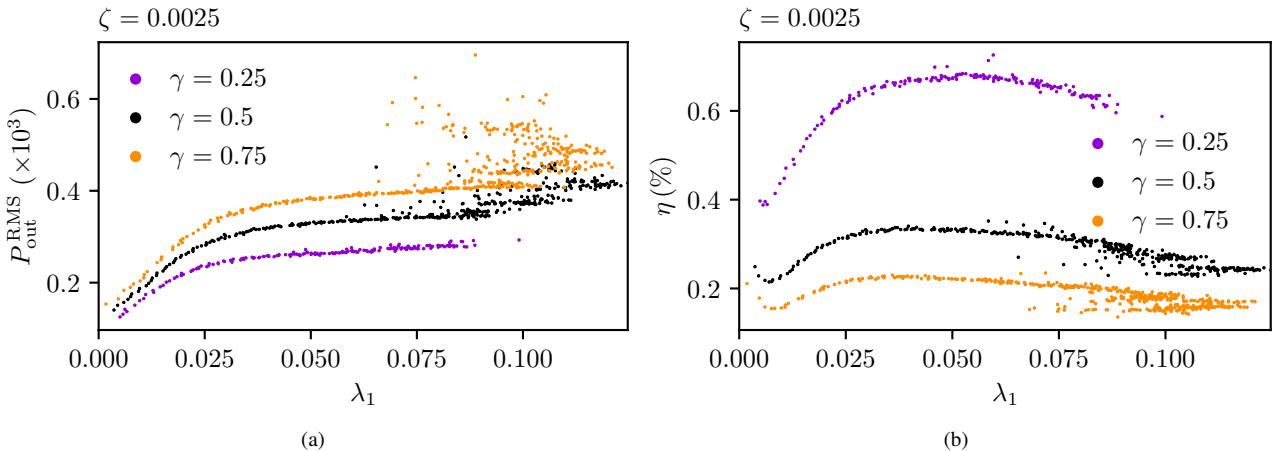Figure 7: Bifurcation diagram for $\zeta = 0.0025$ (a) of λ_1-Ω and (b) η-Ω .

(a)

(b)

Figure 8: Bifurcation diagram for $\gamma = 0.5$ of (a) λ_1-Ω and (b) η-Ω.

Considering the influence of mechanical damping ζ, Fig. 8 displays its influence on both η and λ_1. For $\zeta = 0.025$, $d\eta/d\Omega$ is negative regardless the value of Ω. Hence, as the system approaches the resonance condition ($\Omega \rightarrow 1$), the fraction of dissipated energy by the damper increases. Nevertheless, non intuitively, the efficiency of conversion is higher for low excitation frequency for a higher ζ. Regarding the influence of λ_1, a higher damper tends to decrease λ_1 for any value of excitation frequency Ω.

Now, consider the correlations between the Lyapunov exponents and energy conversion measurements ($P_{\text{out}}^{\text{RMS}}$ and η). Fig. 8a and 8b shows that for damping coefficients of $\zeta = 0.0025$, the correlation between $P_{\text{out}}^{\text{RMS}}$ and λ_1 outputs follows a clear pattern of positive $dP_{\text{out}}^{\text{RMS}}/d\lambda_1$ slope. Around $\lambda_1 = 0.025$ the rate of change starts to quickly decrease, until it reaches a plateau. For $\lambda_1 > 0.06$ the pattern starts to disrupt, getting diffuse and complex, becoming difficult to follow. Additionally, the correlation between η and λ_1 also follows a clear pattern for the same value of damping coefficient ($\zeta = 0.0025$). It starts with a negative slope, until it reaches a local minimum around $0 < \lambda_1 < 0.02$. Then, the slope becomes positive and reaches a peak around $0.025 < \lambda_1 < 0.035$. At last, the slope becomes negative and the pattern start to slowly decrease, reaching a point in which a similar disrupt phenomena occur following the same trend as Fig. 8a. On the other hand, Figures 8c and 8d shows that there is also different correlations for values of $\zeta = 0.025$, however, for that case, the patterns are less concise, indicating the possibility that for greater values of ζ, the correlation patterns tend to be destroyed.

Despite the correlation among energy conversion quantities and the Lyapunov exponent observed in Fig. 8, it is worthwhile mentioning that each point within this figure was generated with a different excitation condition (different Ω), which also contributes to make such quantities to vary. This way, it shows the need of a more rigorous analysis to find a more precise correlation between the energy conversion measurements and the correspondent Lyapunov exponents for chaotic responses.
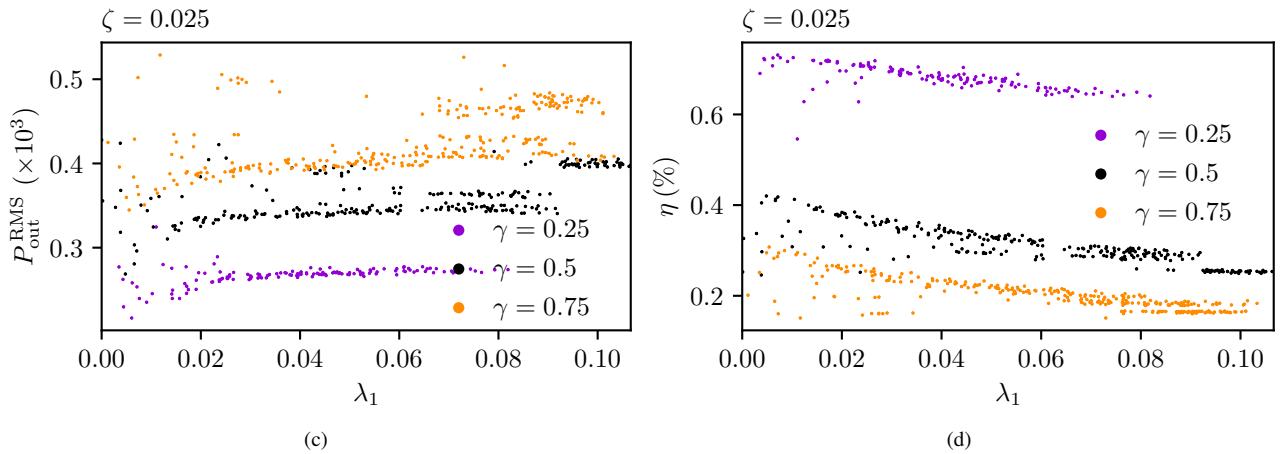

(a)

(b)

Figure 8: Correlations between λ_1 for for $\zeta = 0.025$ and (a) RMS of P_{out}, (b) η for $\zeta = 0.0025$. (c) RMS of P_{out}, (d) η.

5. CONCLUSIONS

This work addresses a numerical analysis of the chaotic responses of bistable piezoelectric energy harvesting device based on the polynomial restitution force model. Results show comprehensive overview diagrams that resumes the chaotic dynamics of the system for a given set of initial conditions based on the equilibrium position of the harvester. Initial analysis show the need to distinguish different patterns of inter-well motion intensity, as it has great influence on the power output of the system. A value of inter-well intensity of 100% was chosen to proceed with the analysis.

A set of bifurcation diagrams were analyzed assigning fixed values for damping and forcing amplitude, and varying the forcing frequency. Main conclusions shows that the magnitude of the largest Lyapunov exponent seems not to be sensitive to the change of the forcing amplitude. Efficiency of the system also is qualitatively the same, changing only its magnitude proportionally with the value of gamma. Also, chaotic responses are always less beneficial compared to the periodic responses, confirming results previously shown in the literature.

Apart from that, correlation plots were made to determine the relation between the energy conversion measurements and the largest Lyapunov exponent. Preliminary results show that there is a clear relationship between P_{out} and λ_1, and therefore η and λ_1. Also, changes in damping change this relation pattern. An observable concerning phenomena representing the destruction of correlation patterns also arise in the analysis, showing that other variables of the system, as excitation frequency, can influence this the correlation, showing the need of a more rigorous analysis in a future work to find a more precise correlation between the electrical outputs and the correspondent largest Lyapunov exponent for chaotic responses.

6. ACKNOWLEDGEMENTS

7. REFERENCES

Bao, B. and Wang, Q., 2021. "A rain energy harvester using a self-release tank". *Mechanical Systems and Signal Processing*, Vol. 147, p. 107099. ISSN 10961216. doi:10.1016/j.ymssp.2020.107099.

Costa, L.G., Monteiro, L.L.d.S., Pacheco, P.M.C.L. and Savi, M.A., 2021. "A parametric analysis of the nonlinear dynamics of bistable vibration-based piezoelectric energy harvesters". *Journal of Intelligent Material Systems and Structures*, Vol. 32, No. 7, pp. 699–723. ISSN 15308138. doi:10.1177/1045389X20963188.

Dagdeviren, C., Yang, B.D., Su, Y., Tran, P.L., Joe, P., Anderson, E., Xia, J., Doraiswamy, V., Dehdashti, B., Feng, X., Lu, B., Poston, R., Khalpey, Z., Ghaffari, R., Huang, Y., Slepian, M.J. and Rogers, J.A., 2014. "Conformal piezoelectric energy harvesting and storage from motions of the heart, lung, and diaphragm". *Proceedings of the National Academy of Sciences of the United States of America*, Vol. 111, No. 5, pp. 1927–1932. ISSN 00278424. doi:10.1073/pnas.1317233111.

Elhalwagy, A.M., Ghoneem, M.Y.M. and Elhadidi, M., 2017. "Feasibility Study for Using Piezoelectric Energy Harvesting Floor in Buildings' Interior Spaces". *Energy Procedia*, Vol. 115, pp. 114–126. ISSN 18766102. doi:10.1016/j.egypro.2017.05.012.

Erturk, A. and Inman, D.J., 2011a. "Broadband piezoelectric power generation on high-energy orbits of the bistable Duffing oscillator with electromechanical coupling". *Journal of Sound and Vibration*, Vol. 330, No. 10, pp. 2339–2353. ISSN 0022-460X. doi:https://doi.org/10.1016/j.jsv.2010.11.018.

Erturk, A., 2011. "Piezoelectric energy harvesting for civil infrastructure system applications: Moving loads and surface strain fluctuations". *Journal of Intelligent Material Systems and Structures*, Vol. 22, No. 17, pp. 1959–1973. ISSN 1045-389X. doi:10.1177/1045389X11420593.

Erturk, A. and Inman, D.J., 2011b. *Piezoelectric Energy Harvesting*. John Wiley & Sons, Ltd, Chichester, UK. ISBN 9781119991151. doi:10.1002/9781119991151.

Ferrari, M., Ferrari, V., Guizzetti, M., Andò, B., Baglio, S. and Trigona, C., 2010a. "Improved energy harvesting from wideband vibrations by nonlinear piezoelectric converters". *Sensors and Actuators, A: Physical*, Vol. 162, No. 2, pp. 425–431. ISSN 09244247. doi:10.1016/j.sna.2010.05.022.

Ferrari, M., Ferrari, V., Guizzetti, M. and Marioli, D., 2010b. "A single-magnet nonlinear piezoelectric converter for enhanced energy harvesting from random vibrations". *Procedia Engineering*, Vol. 5, pp. 1156–1159. ISSN 18777058. doi:10.1016/j.proeng.2010.09.316.

Ilyas, M.A. and Swingler, J., 2015. "Piezoelectric energy harvesting from raindrop impacts". *Energy*, Vol. 90, pp. 796–806. ISSN 03605442. doi:10.1016/j.energy.2015.07.114.

Lee, J. and Choi, B., 2014. "Development of a piezoelectric energy harvesting system for implementing wireless sensors on the tires". *Energy Conversion and Management*, Vol. 78, pp. 32–38. ISSN 01968904. doi:10.1016/j.enconman.2013.09.054.

Nabavi, S.F., Farshidianfar, A. and Afsharfard, A., 2018. "Novel piezoelectric-based ocean wave energy harvesting from offshore buoys". *Applied Ocean Research*, Vol. 76, No. May, pp. 174–183. ISSN 01411187. doi:10.1016/j.apor.2018.05.005.

Noël E. duToit, Brian L. Wardle and Sang-Gook Kim, 2006. "Integrated Ferroelectrics : An MEMS-scale Piezoelectric Mechanical Vibration Energy Havesters". *Taylor & Francis*, , No. November 2012, pp. 121–160.

Paula, A.S.D., Inman, D.J. and Savi, M.A., 2015. "Energy harvesting in a nonlinear piezomagnetoelastic beam subjected to random excitation". *Mechanical Systems and Signal Processing*, Vol. 54-55, pp. 405–416. ISSN 0888-3270. doi:https://doi.org/10.1016/j.ymssp.2014.08.020.

Peigney, M. and Siegert, D., 2013. "Piezoelectric energy harvesting from traffic-induced bridge vibrations". *Smart Materials and Structures*, Vol. 22, No. 9, p. 095019. ISSN 0964-1726. doi:10.1088/0964-1726/22/9/095019.

Pellegrini, S.P., Tolou, N., Schenk, M. and Herder, J.L., 2013. "Bistable vibration energy harvesters: A review". *Journal of Intelligent Material Systems and Structures*, Vol. 24, No. 11, pp. 1303–1312. ISSN 1045-389X. doi:10.1177/1045389X12444940.

Stanton, S.C., McGehee, C.C. and Mann, B.P., 2009. "Reversible hysteresis for broadband magnetopiezoelastic energy harvesting". *Applied Physics Letters*, Vol. 95, No. 17. ISSN 00036951. doi:10.1063/1.3253710.

Tian, W., Shi, Y., Cui, H. and Shi, J., 2020. "Research on piezoelectric energy harvester based on coupled oscillator model for vehicle vibration utilizing a L-shaped cantilever beam". *Smart Materials and Structures*, Vol. 29, No. 7. ISSN 1361665X. doi:10.1088/1361-665X/ab87e1.

Tran, N., Ghayesh, M.H. and Arjomandi, M., 2018. "Ambient vibration energy harvesters: A review on nonlinear techniques for performance enhancement". *International Journal of Engineering Science*, Vol. 127, pp. 162–185. ISSN 00207225. doi:10.1016/j.ijengsci.2018.02.003.

Wang, C., Zhao, J., Li, Q. and Li, Y., 2018. "Optimization design and experimental investigation of piezoelectric energy harvesting devices for pavement". *Applied Energy*, Vol. 229, No. March, pp. 18–30. ISSN 03062619. doi:10.1016/j.apenergy.2018.07.036.

Wolf, A., Swift, J.B., Swinney, H.L. and Vastano, J.A., 1985. "Determining Lyapunov exponents from a time series". *Physica D: Nonlinear Phenomena*, Vol. 16, No. 3, pp. 285–317. ISSN 01672789. doi:10.1016/0167-2789(85)90011-9.

Xiang, H.J., Wang, J.J., Shi, Z.F. and Zhang, Z.W., 2014. "Theoretical analysis of piezoelectric energy harvesting from traffic induced deformation of pavements". *Smart Materials and Structures*, Vol. 23, No. 11, p. 119502. ISSN 0964-1726. doi:10.1088/0964-1726/23/11/119502.

Zhang, Z., Xiang, H., Shi, Z. and Zhan, J., 2018. "Experimental investigation on piezoelectric energy harvesting from vehicle-bridge coupling vibration". *Energy Conversion and Management*, Vol. 163, No. January, pp. 169–179. ISSN 01968904. doi:10.1016/j.enconman.2018.02.054.

Zuo, L. and Tang, X., 2013. "Large-scale vibration energy harvesting". *Journal of Intelligent Material Systems and Structures*, Vol. 24, No. 11, pp. 1405–1430. ISSN 1045-389X. doi:10.1177/1045389X13486707.

8. RESPONSIBILITY NOTICE

The authors are solely responsible for the printed material included in this paper.